CHAPTER 3

EXPERIMENTATION

3.1 RAW MATERIAL

3.1.1 Polymer

In the present study, only high density polyethylene (HDPE) was used.   The characteristics of the HDPE used are shown in Table 3.1.

Table 3.1 Characteristics of the HDPE used (Thai Polyethylene Co.,Ltd.)

Property	Value	
Melt flow rate	5.5	g/10 min.
Density	0.968	g/cm^3
Tensile strength at yield	330	kg$_f$/cm^2
Tensile strength at breakage	200	kg$_f$/cm^2
Elongation at breakage	> 500	%
Stiffness (OLSEN)	12,000	kg$_f$/cm^2
Izod impact strength (with notch)	5	kg$_f$-cm/cm
Hardness (shore D)	66	D scale
Environmental stress cracking resistance	4	F$_{50}$Hr
Melting point	134	^{o}C
Softening point	124	^{o}C
Brittleness temperature	< -80	^{o}C

3.1.2 Pigment

Iron oxide pigments, inorganic pigments, were selected for use in the present study. Generally, they are divided into those of synthetic and natural origins. There are several yellow, brown, red, and black oxides. As a class, they provide inexpensive but dull, lightfast, chemically resistant, non-toxic colors. The natural products are known as ocher, sienna, umber, hematite, and limonite. They include varying amounts of several impurities; in particular, the umber contains manganese.

The synthetic iron oxides are of much higher purity and have less variation in composition. The red iron oxide, Fe_2O_3, has excellent bleed, chemical, heat, and light resistances and is non-toxic. The yellow hydrate, $Fe_2O_3 \cdot x\ H_2O$, is useful up to 175 ^oC, where it loses water and becomes red. Both of these pigments protect resins by screening ultraviolet light. The brown oxide, a mixture of ferrous and ferric oxides, $(FeO)_x(Fe_2O_3)_y$, is useful for producing wood-grain effects in plastics. There are also two mixed oxides, $ZnO \cdot Fe_2O_3$, and $MgO \cdot Fe_2O_3$, that are stable, non-toxic tans.

The natural iron oxides are recommended for use in cellulosics and phenolics, the synthetics for cellulosics, polyethylene, flexible vinyls, and all thermosets. The characteristics of the iron oxide pigments used are shown in Table 3.2.

Table 3.2 Characteristics of the iron oxide pigments used

Property	Pigment A	Pigment B	Pigment C
Loss on heating at 1000 ^oC,1/2 Hr (max. %)	0.6	0.6	1
Sieve residue on 0.045 mm.-mesh (max. %)	0.06	0.06	0.1
Tamped apparent density (g/cm^3)	0.7-1.1	0.7-1.1	1.4-1.8
Density (CA./approx. g/cm^3)	5	5	5
Particle shape	spherical	spherical	spherical
Median particle size (μm)	0.11	0.17	0.2

3.2 EQUIPMENT

The set of experimental equipment was composed of a continuous kneader, an accurate feeder, a press roller, and a roller temperature controller (see their specifications in Appendix A1). A schematic process diagram of the continuous kneading system used in the present study is shown in Figure 3.1
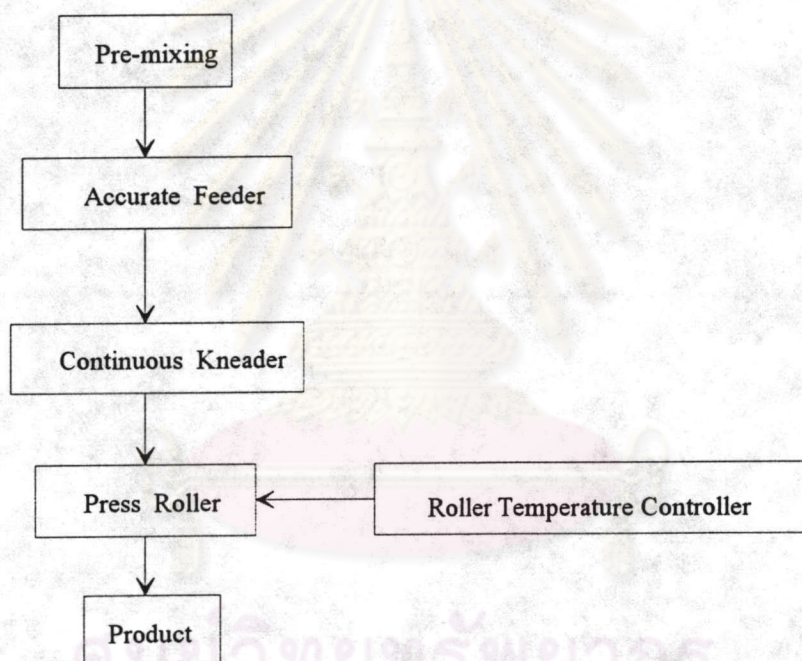

Figure. 3.1   Schematic diagram of the continuous kneading system

3.2.1 Accurate feeder (see Figure 3.2) It handles a wide variety of dry materials including fine powder, granules, chips, pellets, caustics, plastics, food, and pharmaceutical materials. It achieves high rates of accuracy by using a flexible hopper that contorts continuously throughout operation, preventing any bridging of materials inside the hopper, which has been designs to keep all powders flowing downward uniformly with no dead areas, rounded hopper corners to promote material flow, no cracks or seams that would interrupt material flow. The amplitude and frequency of the hopper flexing mechanism are adjustable to gain optimum performance for each material. Metering accuracies generally range between $\pm$ 0.5 to 2 percent for most materials.
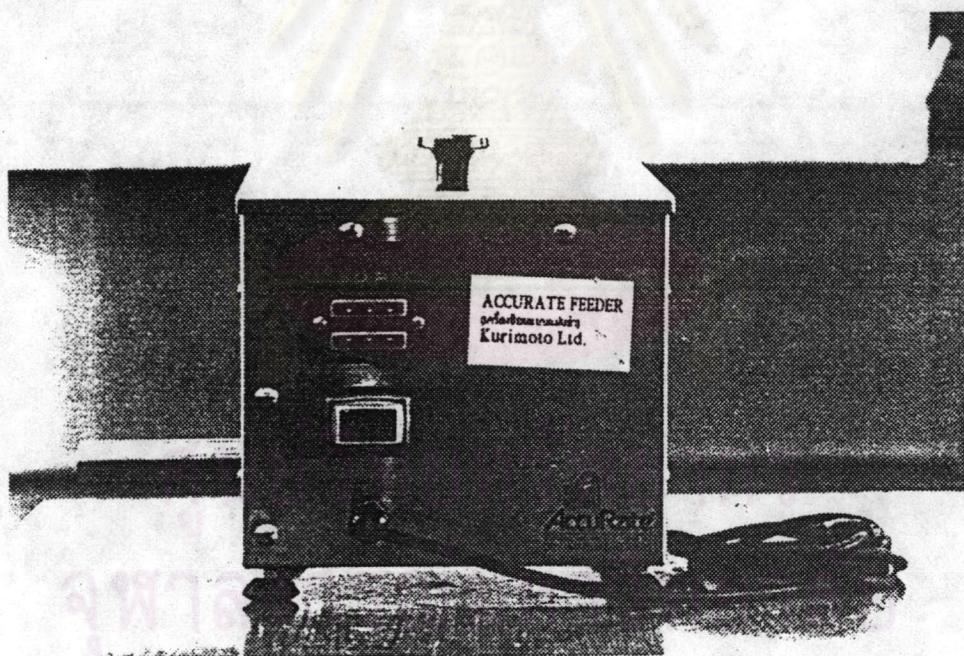

Figure 3.2 Accurate feeder

3.2.2 Continuous Kneader (see in Figure 3.3) It consists of the barrel, screws, paddles, shafts and driving unit.
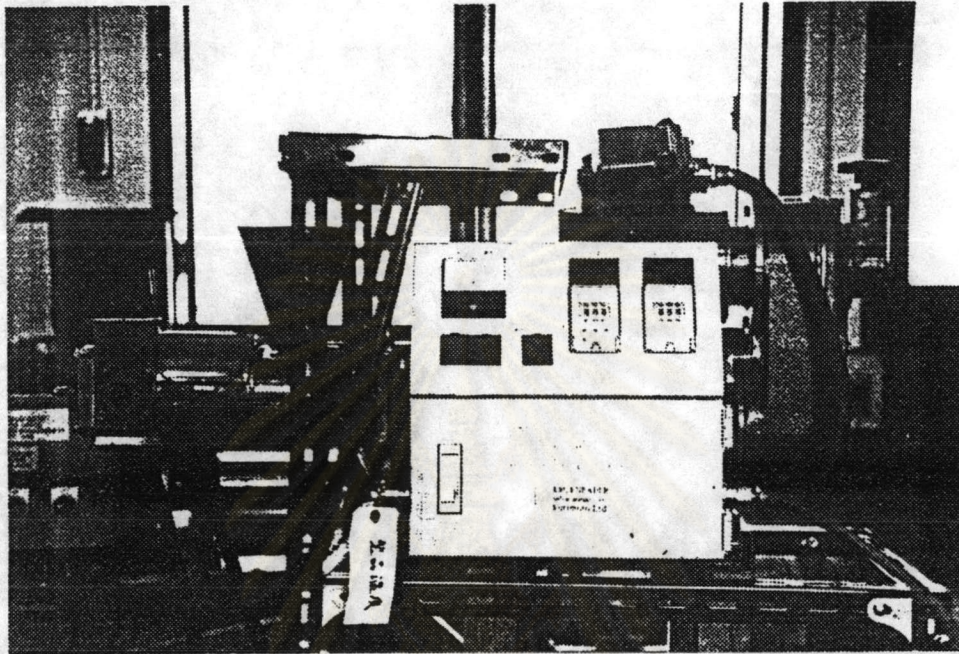

Figure 3.3 Continuous kneader

The barrel is of the horizontally-enclosed type. Material is fed from an inlet at the lower part of one side and discharged from an outlet provided at the upper part on the opposite side (see in Figure 3.4).

Closed type (CL)

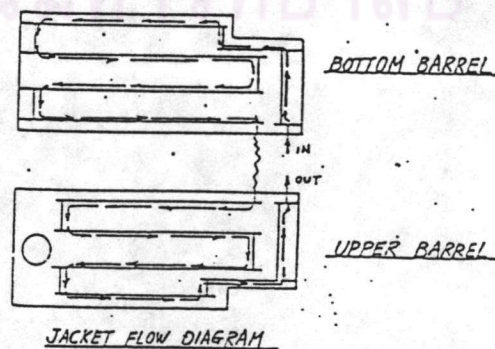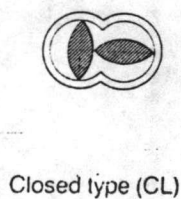BOTTOM BARREL

IN

OUT

UPPER BARREL

JACKET FLOW DIAGRAM

Figure 3.4 Barrel

The paddles and screws are mounted on two sets of horizontal parallel shafts rotating at the same speed and in the same direction (co-rotating). They consisted of five sections, namely, Feed Screw (FS), Helical Paddle (H), Flat Screw (F), Reverse Helical Paddle (RH), and Reverse Screw (RS), as shown in Figure 3.5. The different types of paddles and screws are provided to convey, mix-convey, mix, mix-reverse, and reverse-convey, respectively. The cross-sections of both the paddles and screws are convex. Each type of paddles and screws is further classified into four sub-types according to the key-way angle available in incremental steps of 45° (or 30°) .
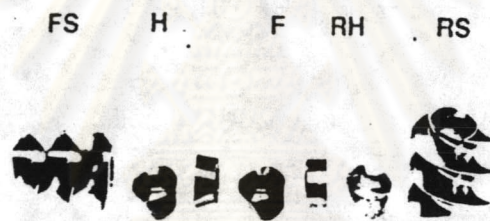
FS   H   F RH   RS

Figure 3.5 Types of paddles and screws

The paddles of one shaft assembly maintain close clearance with the second assembly as well as with the walls of the barrel (see in Figure 3.6). This not only assures a more efficient mixing, but also provides a self-cleaning action for the paddles. The rotation of the two shaft assemblies provides a continual variation in volume between the paddles and the barrel in any given area of the entire unit. At the same time, the action of the shafts also creates an alternating compression and suction of the material. This, in effect, moves the material forward and backward, assuring a continual mixing and re-mixing within any given section. On the other hand, the feed material flows as piston flow and was continuously discharged.
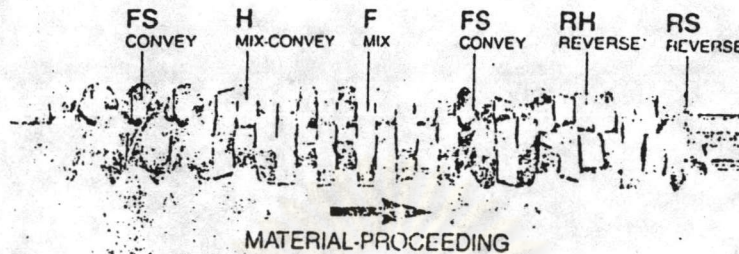
Figure 3.6   The assembly of paddles

To heat or cool the system, a heating-cooling medium is sent through the jackets installed on the upper and lower halves of the barrel. In the present study, ordinary water was used for cooling the barrel and a band heater, for heating. The temperature inside the kneading vessel was measured and used to control the band heater, which was wrapped around the kneading vessel. The heater temperature and kneading vessel inside temperature (hereafter referred to as the kneading temperature) were measured with thermocouples inserted between the heater and kneading vessel, and near the kneading vessel outlet, respectively. The kneading temperature was kept constant via proportional-integral-derivation (PID) control action.

3.2.3   Press Roller (see Figure 3.7) It consists of two parallel rollers rotating in opposite directions and placed close together with the roll axes lying on a horizontal plane, so that a relatively small space or nip exists between the cylindrical surfaces. Material reaching the nip is deformed by friction forces between the material and the rollers and forced to flow through the nip in the direction of the roll motion. Usually, by adjusting the roller temperatures, the material could be made to adhere to either of the rolls as a relatively thin sheet. The

rollers are either heated or cooled by a heating or cooling medium introduced into their respective hollow cores. They are usually rotated at the same speed to facilitate the formation of a sheet.
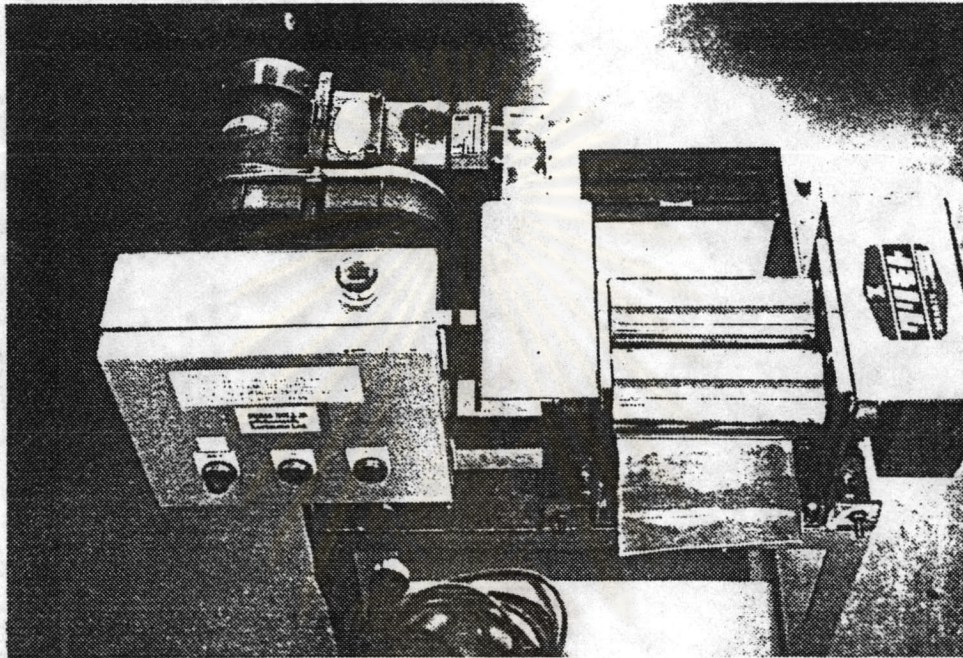

Figure 3.7 Press roller

3.2.4 Roller Temperature Controller (see Figure 3.8) This controller is provided with an advanced temperature control function based on the computer-integrated manufacturing (CIM) system. The CIM system ensures very precise control for either the roller or the medium temperature, responding immediately to any temperature deviation from the set-point.
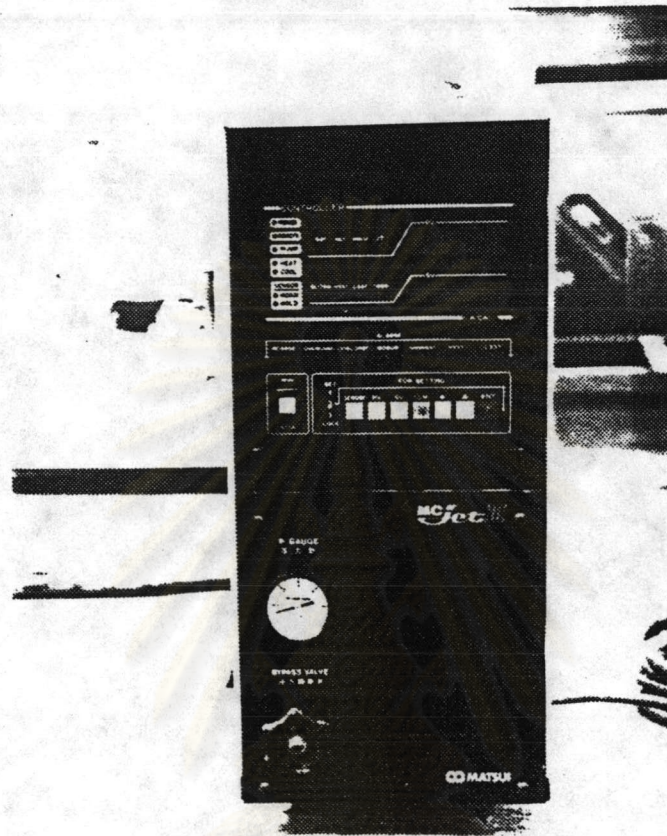
Figure 3.8 Roller temperature controller

3.3 EVALUATION METHODS OF DISPERSIBILITY

The quantitative evaluation of the dispersibility has a few of methods that could be summarized as follows :

ASTM D2663 was the standard test method for carbon-black dispersion in rubber. This method is carried out by measuring the aggregate percentage of the areas covered by pigment particles and agglomerates in microtomed sections of the compound material. According to this method, the compounded rubber is microtomed into sections sufficiently thin to permit observation of the carbon agglomerates by transmitted light, with the aid of a light microscope. The total cross-sectional area of all agglomerates 5 μm. in diameter or larger was counted, and from the known content of carbon black in the stock, the percentage of carbon black below the 5-μm size was calculated. The percentage of carbon black that has been dispersed below the 5-μm agglomerate size, is calculated as follows:

$$\text{Dispersion (\%)} = 100 - SU/L \qquad (3.3.1)$$

where :

U = total number of graticule squares that are at least half filled with carbon black

S = area swelling factor from the action of the solvent used to uncurl the sections

L = volume percentage of carbon black in the compound.

The fractal analysis method represents another group of quantitative methods to evaluate the extent of pigment dispersion. "Fractal" comes from the Latin adjective "fractus", which has the same root as "fraction" and "fragment" and means "irregular or fragmented" (Mandelbrot, 1977). Mathematically a fractal is defined as a geometric shape that is made of parts similar to the whole in the same way, no matter how small it has been subdivided (Sirikalaya, 1994). This means
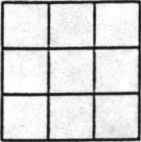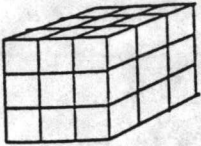
that the shape of a fractal has self-similarity and a fractal dimension. The fractal dimension is a non-integer real number that represents the dimensionality of that fractal. Even an object normally considered as one-dimensional, for example, a line segment, also possesses a self-similar scaling property. The line segment can be divided into N identical parts, each of which is scaled down by the ratio $r = 1/N$ from the whole. Similarly, a two-dimensional object, such as a square area on a plane, can be divided in N self-similar parts, each of which is scaled down by a factor $r = 1/N^{(1/2)}$. A three-dimensional object, such as a solid cube, can be divided in N little cubes, each of which is scaled down by ratio $r = 1/N^{(1/3)}$.

With self-similarity the generalization to fractal dimension is straight-forward. A D-dimensional self-similar object can be divided in N smaller copies of itself, each of which was scaled down by a factor r, where $r = 1/N^{(1/D)}$. Conversely, given a self-similar object of N parts scaled by a ratio r from the whole, as given in Table 3.3, its fractal or similarity dimension is given by:

$$ D = \frac{\log (N)}{\log (1/r)} = -\frac{\log (N)}{\log (r)} \qquad (3.3.2)$$

In other words, the fractal is defined as an extremely irregular line (or surface) formed of an infinite number of similarly irregular sections (or parts). The fractal had fractional dimension between one and two (or between two and three). It could be shown that an extremely irregular shape might be treated as a fractal, for example, the coastline (shoreline) of a country.

Table 3.3 Scaling law for fractional dimension (Sirikalaya, 1994)

Object	Number of pieces (N)	Scaling (r)	Law
	3	1/3	$3 = 3^1$
	9	$1/3^{(1/2)}$	$9 = 3^2$
	27	$1/3^{(1/3)}$	$27 = 3^3$

Let   N(r) be the counted number of subsections (squares of side *r*) containing at least one small part of a fractal when the representative length of each subsection was *r* , *r* = 1/n (n = number of division to similarity), the so-called similarity ratio.

For the fractal, the following equation holds:

$$N(r) = (\text{Similarity ratio})^{-D} = (r)^{-D} \qquad (3.3.3)$$

Thus the fractal dimension, D, is defined by :

$$D = -\frac{\log N(r)}{\log r} \qquad (3.3.4)$$

In the fractal analysis of pore shape (Sirikalaya, 1994), the cut specimens were micro-photographed using a reflecting microscope. An illustration of the count N(r) versus the similarity ratio r is shown in Figure 3.9.
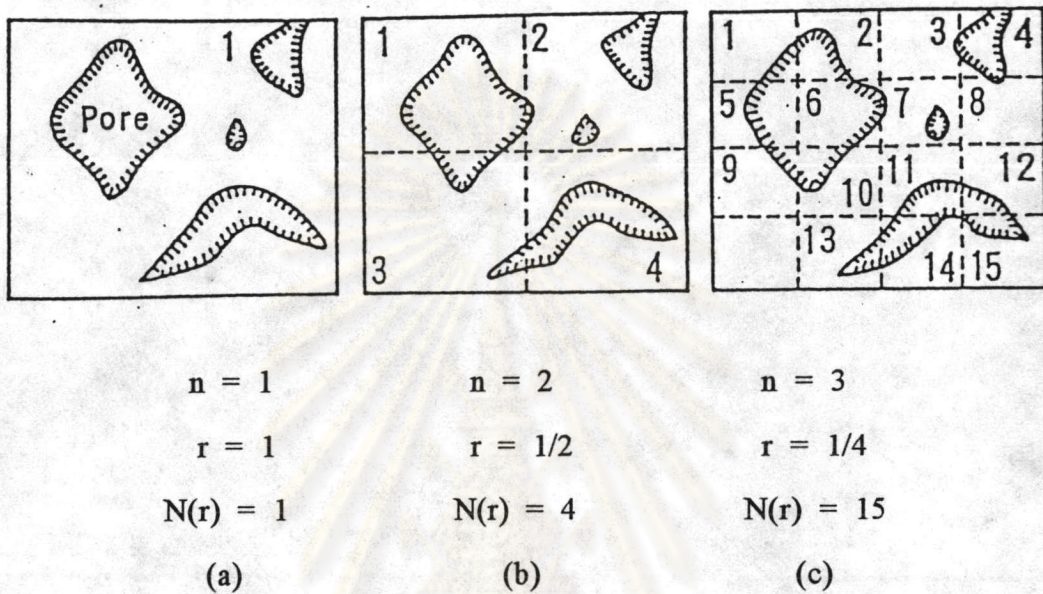

n = 1   n = 2   n = 3

r = 1   r = 1/2   r = 1/4

N(r) = 1   N(r) = 4   N(r) = 15

(a)   (b)   (c)

Figure 3.9 Determination of fractal dimension (Sirikalaya, 1994)

The observed relationship between N(r) and r was plotted on the log-log scale, and the fractal dimension was calculated from the slope of the convergent straight lines in Figure 3.10.
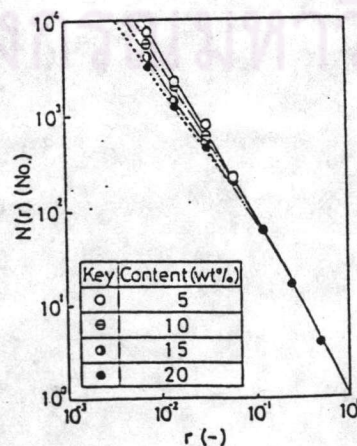

Figure 3.10 Example of fractal dimension determination (Sirikalaya, 1994)

Terashita, et.al.(1993) are among the first researchers to apply the fractal analysis concept to evaluate the dispersion state. Their detailed observations of large number of minute samples to determine the fractal dimension were greatly aided with the use of an image analyzer. A schematic diagram of the image analyzer system is shown in Figure 3.11.
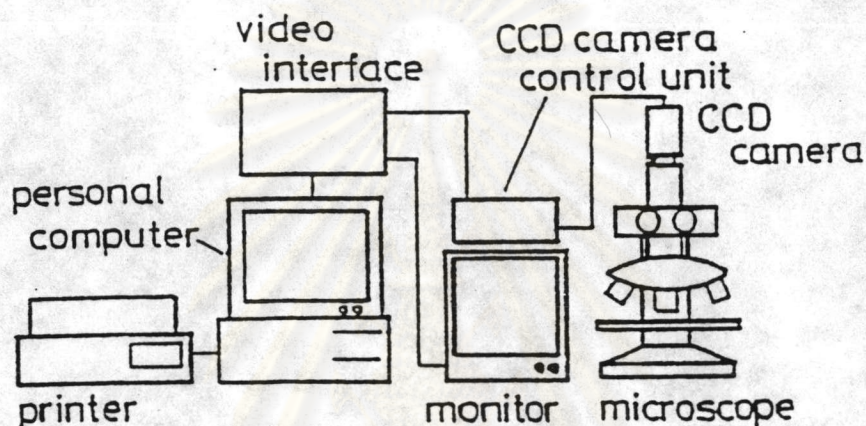

Figure 3.11 A schematic diagram of the image analyzer (Terashita, 1993)

Each sample was observed using light microscopy, and the obtained image was photographed using a CCD camera. The analog signal from the CCD camera was digitized and sent to a computer via a video interface. The obtained digital information was subjected to a smoothing treatment to remove noise before being converted to binary data to locate the particle-containing region on the image. After these processings, the image was displayed on a CRT screen and used to calculate the fractal dimension. In this analysis, the magnifying power should be optimized to enable observation of the particle distribution over as wide a range as possible. Based on this dealt image, the fractal dimension was to be determined as a quantitative representation of the dispersion state, as follows:

First, the dealt image was divided into n x n segments ($2 \leq n \leq 80$) to yield n^2 segments. Next, for each segment, the area ratio S_f of pigment particles was calculated as follows:

$$S_f = A_f / A \tag{3.3.5}$$

where A_f was the area occupied by the particles in a single segment, and A was the total area of the same segment. A coefficient of variance $Ds(n)$ was calculated from the mean value of S_f for an arbitrary n (namely $\overline{S}_f(n)$) and the standard deviation $\sigma s(n)$ as follows

$$Ds(n) = \sigma s(n) / \overline{S}_f(n) \tag{3.3.6}$$

Next $Ds(n)$ versus $1/n$ was plotted on a log-log scale, and if $Ds(n)$ and $1/n$ bears the relationship :

$$Ds(n) \; \alpha \; (1/n)^{-D} \tag{3.3.7}$$

then the particle dispersion state could be characterized by the fractal dimension (D).

Since linearity was observed over the range of $2 \leq n \leq 80$, as shown in Figure 3.12, the fractal dimension (D) could be calculated from the slope. Naturally, the particle dispersion state improved as D increased.
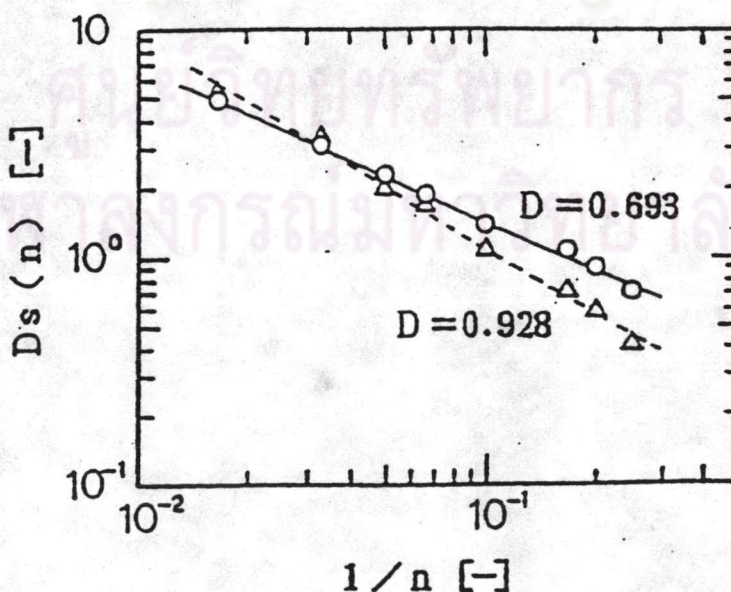
Figure 3.12 Example of calculation of fractal dimension (Terashita, 1993)

Figure 3.13 depicts two dealt images showing the filler dispersion state and its fractal dimension (D). In this figure, black spots and lines indicate fillers, while the white portions indicate the matrix resin. A high value of the fractal dimension demonstrated a visually good dispersion state with little filler aggregation. In other words, the fractal dimension proved useful in quantitative determination of particle dispersion state.

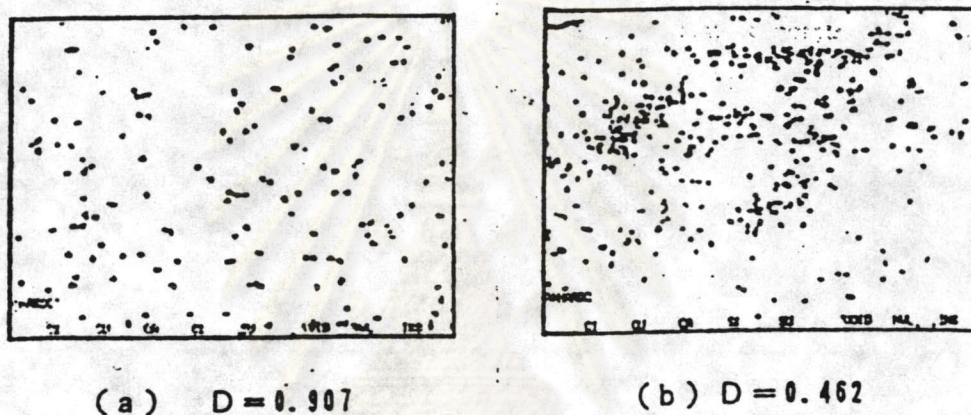

(a)   D = 0.907   (b) D = 0.462

Figure 3.13 Dealt image showing filler dispersion state and its fractal dimension(D)

(Terashita, 1993)

In the present study, the pigment used was iron oxide so the dispersibilty could not be evaluated by ASTM D2663 which is only suitable for carbon black. The fractal analysis method was thus chosen to evaluate the dispersibility in the present study. Since the used pigments were very small in size (0.11 μm. to 0.20 μ m. median sizes) and the wave-length of visible light was broader than the pigment size, micro-photograph would not be applicable, and light microscopy coupled with image analyzer was not suitable for use in the present study.

However, dispersibility in the present study was still evaluated by the fractal analysis concept. All prepared samples were micro-photographed using a scanning electron microscope (SEM). The used magnifying power was 5000X, operated at

20 KeV beam current. Then each micro-photograph was divided in nxn subsections (n = 2, 4, 5, 8, 10, 20, 40, and 80) and the number of subsections containing at least some part of any pigment particle, N(r), was counted at each similarity ratio (r). The relation between N(r) versus r was plotted on log-log scale to calculate the slope of the convergent straight line, which gives the fractal dimension.

A complete setup of the continuous kneading system in the present study is shown in Figure 3.14.
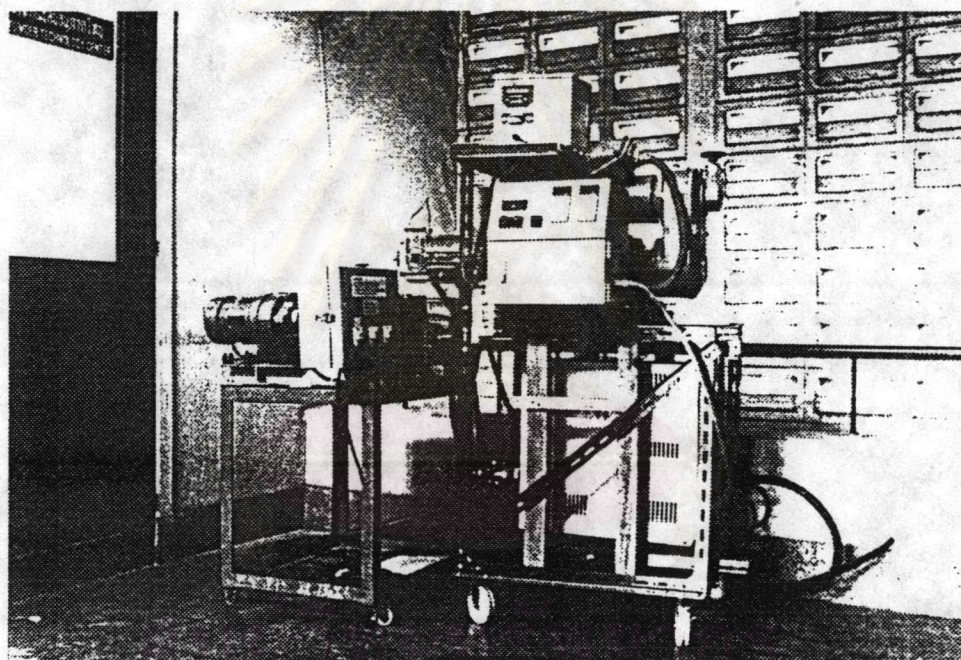

Figure 3.14 The continuous kneading system in the present study

3.4 EXPERIMENTAL PROCEDURE

The experimental procedure is as follows :

1. Premix polyethylene and pigment at a constant ratio (25:1 by weight) a using V blender for approximately 5 minutes.

2. Set the flow rate of the accurate feeder at a constant rate of 34 g/min. (potentiometer no. = 500)

3. Set the rotational speed of the press roller at a constant speed of 2 rpm.

4. Set kneading conditions (kneading temperature, roller temperature, rotational speed of screw) at the desired conditions.

5. Wait until the kneading conditions reach steady-state conditions.

6. Start to feed the mixed material from the feed hopper of the accurate feeder at the constant rate to the kneading vessel inlet.

7. Discharge the kneaded mixture from the kneader outlet onto the press roller to press the kneaded mixture into a long thin plate (about 0.10 mm. thick).

8. After each experimental run had been completed, feed the PE resin alone to the kneading vessel to purge out any remaining material before starting a new experimental run.

9. To evaluate the resulting dispersibility, microphotograph a total of 4 samples of the thin plate from each run with the aid of a scanning electron microscope (SEM) at magnifying power 5000X, 20 KeV.

10. Analyze the SEM photographs with the fractal analysis method using the following number of division to similarity (n) : 2, 4, 5, 8, 10, 20, 40 and 80. In other words, the similarity ratios (r) are 1/2, 1/4, 1/5, 1/8, 1/10, 1/20 ,1/40 and 1/80, respectively.

11. Count the number of similarity parts , N(r), that contain at least some small part of a pigment particle or agglomerate.

12. Plot N(r) versus r on a log-log scale to determine the fractal dimension (D).